ADVANCED FUNCTIONAL MATERIALS
www.afm-journal.de

Photon Energy-Dependent Optical Spin-Orbit Torque in Heavy Metal–Ferromagnet Bilayers

*Chuangtang Wang, Yihao Xu, and Yongmin Liu**

The manipulation of magnetization through optically generated ultrafast spin currents is a fascinating area that needs a thorough understanding for its potential future applications. In this work, a comprehensive investigation of helicity-driven optical spin-orbit torque in heavy metal/ferromagnetic metal heterostructures is presented, specifically cobalt capped with gold or platinum, subject to laser pumping at different wavelengths. The results demonstrate up to tenfold enhancement in optical spin-orbit torque quantum efficiency for gold compared to platinum of the same thickness when pumped with a visible laser. Additionally, the study provides the first experimental analysis of the photon energy dependence of optical spin-orbit torque and derives the optical spin orientation spectra for both gold/cobalt and platinum/cobalt heterostructures. A key insight gained from the study is the impact of photon energy-dependent spin transport in the system, which suggests the use of a high photon energy pump for efficient spin transport. These findings highlight the potential of spin current generation and manipulation in gold/ferromagnet heterostructures for a wide range of applications such as all-optical magnetization switching, spin-wave generation and control, and spintronic terahertz emission.

1. Introduction

Applying femtosecond lasers, known as one of the most potent stimuli, to control magnetic materials has led to the emergence of ultrafast magnetism.[1] Within this research domain, the optically generated ultrashort spin current stands out as a particularly captivating subject for investigation. For example, superdiffusive spin-current transport in nonmagnetic metal/ferromagnetic metal heterostructures has been demonstrated to play a pivotal role in ultrafast demagnetization processes.[2] The spin-majority electrons, which possess higher velocities and longer lifetimes compared to their spin-minority counterparts, traverse the interface while the spin-minority electrons remain confined within the ferromagnets, resulting in ultrafast demagnetization.[3] This ultrafast demagnetization-driven spin current can also be converted into a charge current via the inverse spin Hall effect, and generate terahertz (THz) electric field emission.[4] Such spintronic THz emitters exhibit a broad THz spectrum, considerable amplitude, and excellent tunability by means of external magnetic[5] or electric fields,[6] rendering them promising candidates for future THz emitter applications. Furthermore, the spin currents emanating from the demagnetization of one layer can be harnessed and employed to drive the magnetization precession of another layer.[7] Notably, these spin currents possess sufficient magnitude to induce single-pulse switching of ferromagnet magnetization,[8] a result that typically requires accumulative pulses for successful execution.[9]

Different from demagnetization-driven spin current, an alternative source of spin current generation originates from optical orientation. This process involves circularly polarized laser pulses directly transferring their angular momentum in accordance with optical selection rules, thereby generating spin-polarized carriers within a given material.[10] This phenomenon has been predominantly investigated in semiconductor materials, such as gallium arsenide (GaAs).[11] In the case of ferromagnetic semiconductors, such as gallium manganese arsenide ((Ga,Mn)As), these spin-polarized carriers interact with the ferromagnetic moments of manganese via exchange coupling, thereby facilitating optical spin-transfer torque and providing a novel avenue for magnetization control.[12] Optical spin-orbit torque (OSOT) was also demonstrated afterward in (Ga,Mn)As.[13] Nevertheless, ferromagnetic semiconductors are hindered by the constraint of low Curie temperatures. Consequently, the development of new strategies to control optical torques in metallic materials with high Curie temperatures becomes a pressing task that demands further exploration.

The helicity-dependent interaction between light and magnetic metals has been extensively investigated in the context

C. Wang, Y. Liu
Department of Electrical and Computer Engineering
Northeastern University
Boston, MA 02115, USA
E-mail: y.liu@northeastern.edu
Y. Xu, Y. Liu
Department of Mechanical and Industrial Engineering
Northeastern University
Boston, MA 02115, USA

The ORCID identification number(s) for the author(s) of this article can be found under https://doi.org/10.1002/adfm.202307753

DOI: 10.1002/adfm.202307753

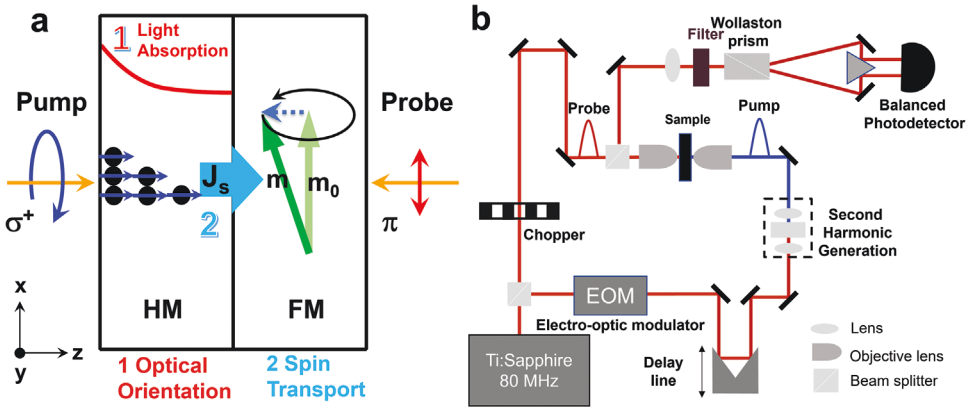

Figure 1. Schematics of optical spin-orbit torque and experimental setup. a) Schematic for optical spin-orbit torque in a heavy metal (HM)/ferromagnetic metal (FM) heterostructure. Right-handed circularly polarized (σ^+) pump light is absorbed by the HM layer and generates spin carriers (filled black circles with solid blue arrow indicating the spin angular momentum direction) through optical orientation process. The spin carriers then diffuse from the HM to the FM in the form of spin currents (J_s), which exert a torque on the FM and induce magnetization precession. The green arrows indicate the equilibrium magnetization direction along the *x*-axis (m_0) and transient magnetization direction (m), and the dashed blue arrow indicates the optical spin-orbit torque direction. A linearly polarized light (π, red arrow) is used to probe the magnetization dynamics. b) Schematic illustration of time-resolved magneto-optical Kerr effect spectroscopy used in this work.

of all-optical switching of magnetization.[14] Heavy metal (HM)/ferromagnetic metal (FM) heterostructures constitute the cornerstone of spintronic devices, yet the all-optical control of magnetization in such structures has been relatively underexplored.[9] Only a limited number of studies have been conducted on helicity-driven spin currents and torques in HM/FM heterostructures.[15] Upon the interaction of circularly polarized light with in-plane magnetized HM/FM heterostructures, three distinct torques can be exerted on the FM. The first one is OSOT, wherein spin-polarized carriers are first generated in the HM by optical orientation with a spin polarization efficiency of P_s. Then, the spin-polarized carriers diffuse into the FM layer and induce a damping-like torque on the FM with a spin collection efficiency of P_c[15a,c] as shown in **Figure 1**a. Consequently, we have an overall OSOT quantum efficiency $\eta = P_s P_c$. Please note that we follow the terminology of OSOT defined by Choi et al.,[15c] considering its structure analogy to electric spin-orbit torque in an HM/FM bilayer. Additionally, an in-plane field-like optical torque emerges in HM/FM heterostructures as a consequence of the optical Rashba–Edelstein effect.[15d] Lastly, the FM can directly interact with light through the inverse Faraday effect (IFE), resulting in the generation of a field-like torque.[15a] OSOT is found to be the dominant torque in HM/FM heterostructures and presents itself as a potentially viable approach for controlling the magnetization of thin film magnets. Nevertheless, our current understanding of OSOT in HM/FM heterostructures remains limited. Previous investigations were conducted with a single photon energy,[15a,c-e] and a comprehensive analysis of the photon energy dependence of OSOT in HM/FM heterostructures is still lacking. For example, the dependence of optical orientation on photon energy has not been studied. On the other hand, whether spin transport is affected by photon energy remains unexplored. These subjects are essential to better understand the underlying physics and maximize OSOT for practical applications. Additionally, heavy metals such as platinum (Pt), palladium (Pd), tungsten (W), and tantalum (Ta) have been selectively studied owing to their substantial spin-orbit coupling strength, as investigated in spintronics.[15c] Gold (Au) has also been examined, albeit exhibiting minimal OSOT under near-infrared light pump conditions.[15e]

In this work, we report the observation of a surprisingly large OSOT quantum efficiency in Au when exposed to visible light pumping. We systematically investigate the photon energy-dependent OSOT in cobalt (Co) capped with Au and Pt. Our findings offer valuable insights into the optical orientation of heavy metals and the mechanisms of energy-dependent spin transport. The results suggest that enhanced optical orientation and more efficient spin transport occur when utilizing laser excitation with high photon energy. These intriguing results provide guidance on the potential use of heavy metal Au and visible pump lasers, as opposed to the more commonly employed near-infrared lasers, for future opto-magnetic applications.

2. Results and Discussion

2.1. Experiment

Thin film structures consisting of sapphire/Pt(d_{Pt})/Co(5)/SiO_2(3) and sapphire/Au(d_{Au})/Co(5)/SiO_2(3) were fabricated by magnetron sputtering, with the numbers in parentheses denoting the respective thicknesses in nanometers. In these structures, sapphire serves as the substrate, while d_{Pt} and d_{Au} represent the thicknesses of Pt and Au, respectively. A SiO_2 layer with a thickness of 3 nm was deposited to inhibit the oxidation of Co. The magnetization dynamics induced by OSOT was characterized by a home-built time-resolved magneto-optical Kerr effect (MOKE) spectroscopy system based on a tunable Ti:sapphire oscillator, as depicted in Figure 1b. The thin film structures were pumped from the sapphire substrate side and probed from the opposite side in a polar MOKE configuration, with an external magnetic field applied along the direction parallel to the sample plane. The pump light was circularly polarized and the probe light was linearly polarized. In this study, we employed a two-color configuration, utilizing the fundamental light from the

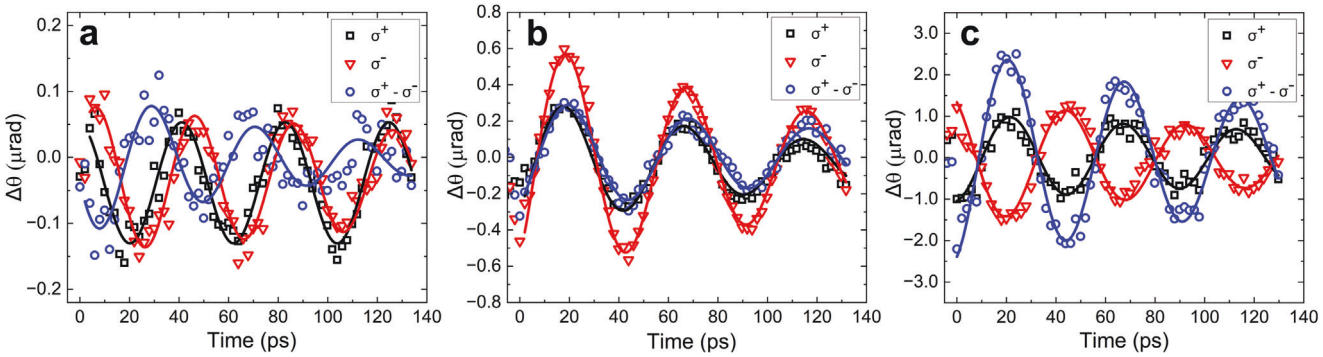

Figure 2. Magnetization dynamics induced by optical spin-orbit torque. Magnetization dynamics excited by right-handed (σ^+) and left-handed (σ^-) circularly polarized light with a wavelength of 400 nm in a) sapphire/Co(5)/SiO_2(3), b) sapphire/Pt(3)/Co(5)/SiO_2(3), and c) sapphire/Au(10)/Co(5)/SiO_2(3) samples. The external magnetic field is around 2800 Oe, corresponding to an oscillation frequency of 20.5 GHz. The difference between σ^+ and σ^- shows only helicity-dependent magnetization dynamics. It helps to eliminate the contribution of the reflection background arising from an imperfect photodetector balancing and nonsymmetric magnetization dynamics under σ^+ and σ^- illumination due to the possible misalignment of the external magnetic field and magnetic easy-anisotropy axis (See Figure S1, Supporting Information and the discussion in Section S1, Supporting Information).

Ti:sapphire laser (ranging from 800 to 1040 nm) as the pump and its corresponding second harmonic generation light (spanning from 400 to 520 nm) as the probe, or vice versa. We conducted thickness dependence measurements of OSOT with a 400 nm pump (photon energy of 3.1 eV) for both d_{Pt} and d_{Au}. Samples of sapphire/Pt(3)/Co(5)/SiO_2(3) (hereafter denoted as Pt3Co5) and sapphire/Au(10)/Co(5)/SiO_2(3) (hereafter denoted as Au10Co5) were utilized to assess the photon energy dependence of OSOT.

2.2. Thickness Dependence of OSOT

We characterized the dynamics of the z-component of magnetization of different samples pumped with right-handed (σ^+) and left-handed (σ^-) circularly polarized light, and helicity-dependent magnetization dynamics was deduced by subtracting the σ^+ and σ^- cases. **Figure 2** displays three representative samples of Co (5 nm), Pt3Co5, and Au10Co5. The magnetization dynamics can be fitted with a damped cosine function: $A\cos(2\pi ft - \phi)\exp(-t/\tau)$, where A, f, ϕ, and τ represent the amplitude, frequency, initial phase, and lifetime of magnetization precession, respectively. In the scenario of ferromagnetic Co with in-plane anisotropy and an in-plane external magnetic field, the magnetization m aligns along the in-plane direction. When the magnetization is excited by the in-plane IFE-generated field-like torque $\boldsymbol{m} \times \boldsymbol{\sigma}$, where $\boldsymbol{m}$ and $\boldsymbol{\sigma}$ are the magnetization and angular momentum of circularly polarized light, the magnetization is instantaneously tilted toward another in-plane direction, followed by damped magnetization precession governed by the Landau–Lifshitz-Gilbert equation. Under polar MOKE geometry, ϕ will be 90° without out-of-plane tilt. Conversely, OSOT-generated damping-like torque $\boldsymbol{m} \times (\boldsymbol{m} \times \boldsymbol{\sigma})$ is oriented along the out-of-plane direction, and the corresponding ϕ will be 0°. For a bare Co thin film, IFE-torque dominates, and thus the magnetization dynamics does not exhibit a substantial out-of-plane tilt as indicated by $\phi = 72°$ (Figure 2a). In the cases of Pt3Co5 and Au10Co5, however, both exhibit a dominated out-of-plane tilt at the starting time of pumping. The dynamics responses are better fitted with a cosine function with $\phi = 36°$ and 20° respectively, as shown in Figure 2b,c. Interestingly, at the employed photon energy of 3.1 eV, Au functions as a more potent OSOT source compared to Pt since the amplitude of magnetization dynamics is four times larger in Au10Co5. We further quantify the OSOT quantum efficiency, which is defined as

$$\eta = \frac{\Delta M \cdot d_{Co}}{\mu_B} \Big/ \frac{F_{in} \cdot Abs}{\hbar\omega} \tag{1}$$

Equation (1) represents the percentage of absorbed spin angular momentum from photons (that is, $\frac{F_{in} \cdot Abs}{\hbar\omega}$) converted into the spin angular momentum transferred into Co (that is, $\frac{\Delta M \cdot d_{Co}}{\mu_B}$). Here ΔM is computed by comparison with the static MOKE angle, d_{Co} is the thickness of Co, and μ_B denotes the Bohr magneton. F_{in} refers to the laser fluence used in this work, which is 6 J m^{-2}. Abs denotes the absorption percentage of Pt or Au, and $\hbar\omega$ represents the photon energy. The calculated η for 3 nm Pt is 0.015, which is in close agreement with the reported values.[15c-e] Surprisingly, η is 0.11 in the instance of 10 nm Au capping, although Au has not been commonly used to produce OSOT. This result motivates us to investigate the OSOT process more closely.

Based on the theory proposed by Choi et al. for HM/FM bilayers [15c] and the photo-induced inverse spin Hall effect theory in Pt/semiconductor junctions,[16] the OSOT process involves two steps: spin generation in HM and diffusion of carriers toward the interface. One plausible explanation for the enhanced η in the Au10Co5 sample is that Au has a longer spin diffusion length (L_s) compared to Pt, as reported in the literature.[17] It indicates that more spins survive across the HM/FM interface before they are scattered. We quantify the spin diffusion length of Au and Pt in our case by measuring the thickness-dependent η in Au and Pt. Then we fit the results using a spin diffusion model by numerically solving the spin diffusion equation:[7b,15e,18]

$$\frac{\partial \mu_s}{\partial t} = D\frac{\partial^2 \mu_s}{\partial z^2} - \frac{\mu_s}{L_s^2/D} + P_s \frac{2a(z)\, F_{in}}{\hbar\omega N_F} G(t) \tag{2}$$

Here μ_s, D, $a(z)$, N_F and $G(t)$ represent the spin chemical potential, diffusion constant, light absorption profile inside the heavy

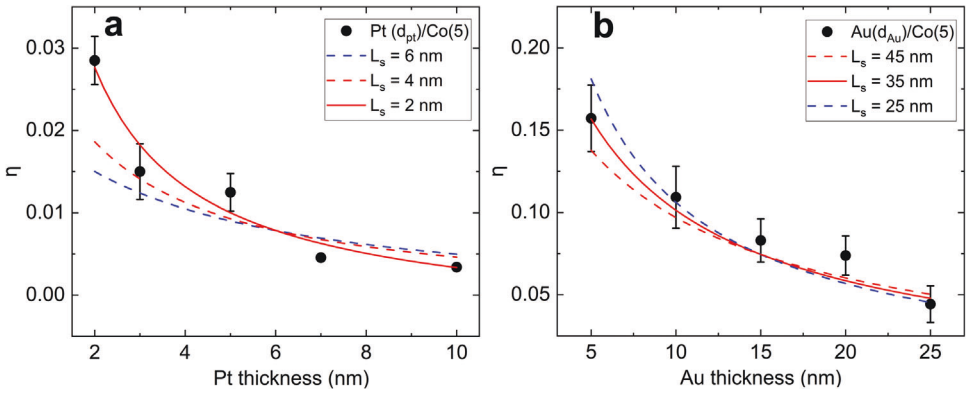

Figure 3. Thickness-dependent optical spin-orbit torque quantum efficiency (η). η of a) sapphire/Pt(d_{Pt})/Co(5)/SiO_2(3) and b) sapphire/Au(d_{Au})/Co(5)/SiO_2(3) samples under the pump photon energy of 3.1 eV. The dots are the experimental data, and the solid curves represent the best-fitted result from the spin diffusion simulation by varying the spin diffusion length (L_s). The other two dash curves are normalized to the best-fitted results to illustrate the trend difference with different spin diffusion length.

metal, spin density of states at the Fermi level, and temporal profile of the Gaussian laser pulse, respectively. Please note that the spin relaxation time (τ_s) is related to L_s by $\tau_s = L_s^2 / D$. The results are presented in **Figure 3**a,b, while the unnormalized data are plotted in Figure S2 (Supporting Information). In both cases, η decreases as the thickness increases, which is expected since spins experience more scattering as they travel a longer distance. Note that η of Au is one order larger than Pt with the same thickness. For example, η is 0.157 and 0.012 for 5 nm Au and Pt, respectively. The simulated thickness-dependent η with varying L_s are plotted alongside the experimental data. Based on the similar trend between the experimental and simulation results, we can determine that the spin diffusion length is 2 nm for Pt and 35 nm for Au, which are within the range of previously reported values (1–10 nm for Pt and 30–100 nm for Au).[17]

2.3. Photon Energy Dependence of OSOT

As mentioned in the introduction, the overall OSOT quantum efficiency is given by $\eta = P_s P_c$. The longer spin diffusion length alone cannot account for the significantly larger η observed in Au. From the spin diffusion model (see Experimental Section), we deduce the value of P_c to be 0.6 for Au10Co5, while P_c is 0.18 for Pt3Co5. Conversely, prior research has indicated that η of Au under near-infrared pump illumination is relatively weak.[15e] Therefore, investigating the photon energy dependence of OSOT is essential to fully understand this unusual phenomenon. We have conducted measurements of pump photon energy-dependent OSOT in Pt3Co5 and Au10Co5 samples, and the results are presented in **Figure 4**a,b, respectively. The original data of magnetization dynamics can be found in Figure S3 (Supporting Information). For all the tested photon energies, the Pt3Co5 sample exhibits OSOT-dominated magnetization dynamics with substantial transient out-of-plane tilt. As demonstrated in Figure 4c, the OSOT increases as photon energy decreases from 3.10 to 1.44 eV, while exhibiting diminished efficiency with even lower photon energies. In the case of Au10Co5, the difference between the near-infrared pump and the visible pump is significant. When the photon energy is >2.5 eV, OSOT-dominated magnetization dynamics are observed. However, with lower photon energies, the magnetization dynamics show IFE-dominated characteristics with large ϕ, and the amplitude is considerably smaller than that in the OSOT case. The

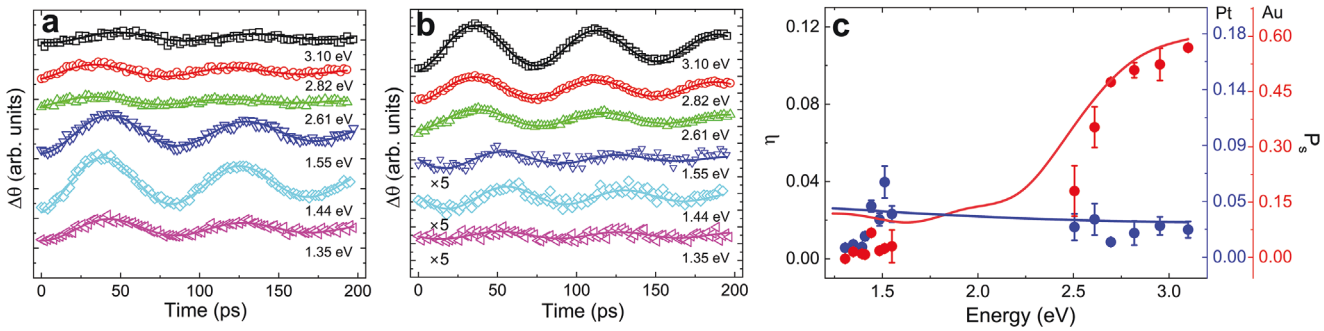

Figure 4. Photon energy-dependent optical spin-orbit torque. Magnetization dynamics under different photon energy excitations in a) sapphire/Pt(3)/Co(5)/SiO_2(3) and b) sapphire/Au(10)/Co(5)/SiO_2(3) samples. The external magnetic field is around 1200 Oe, corresponding to an oscillation frequency of 12.9 GHz. c) Measured optical spin-orbit torque quantum efficiency η of the sapphire/Pt(3)/Co(5)/SiO_2(3) sample (blue dots) and sapphire/Au(10)/Co(5)/SiO_2(3) sample (red dots). The blue and red solid lines are the derived η for Pt and Au samples, respectively, based on the simulated spin collection efficiency using the spin diffusion model. The right column of c shows the derived optical spin polarization efficiency (P_s).

decrease in OSOT amplitude is expected, because the absorption substantially reduces when the photon energy falls below the interband transition gap of 2.5 eV for Au. The details for wavelength-dependent absorption of heavy metals in Pt3Co5 and Au10Co5 can be found in Figure S4 (Supporting Information). Intriguingly, η exhibits the same decreasing trend with reduced photon energy. It is important to note that η is a normalized quantity relative to absorption, as evidenced by the definition of η in Equation (1).

We have examined photon energy-dependent P_c. In the case of the semiconductor junctions previously studied (e.g., GaAs/Pt, Ge/Pt, and Si/Pt), a 1D analytical diffusion model successfully reproduces the optical orientation and spin transport behavior, despite the differences in the band structures among GaAs, Ge, and Si.[16] The photon energy dependence of η exhibits the following proportionality relation: $\eta \propto P_s P_c \propto \frac{P_s(\hbar\omega)\alpha(\hbar\omega)L_s}{1+\alpha(\hbar\omega)L_s}$, where α represents the absorption coefficient. If the absorption length $L_\alpha = 1/\alpha$ is significantly greater than L_s (or $\alpha L_s \ll 1$), the spin-polarized carriers will undergo dephasing before reaching the interface, and hence $\eta \propto P_s(\hbar\omega)\alpha(\hbar\omega)L_s$. If L_α is much smaller than L_s (or $\alpha L_s \gg 1$), spin-polarized carriers enter the FM before dephasing, causing the photon energy dependence of OSOT to be dominated by $P_s(\hbar\omega)$. As demonstrated in Equation (2), our spin diffusion model explicitly incorporates the contributions of L_α in the $a(z)$ term and L_s. We have directly simulated photon energy-dependent P_c considering the dispersion of refractive index of materials (see Figure S5, Supporting Information). The Pt3Co5 and Au10Co5 samples both exhibit minor weak photon energy dependence. For Pt3Co5, L_α is ≈10 nm across the studied photon energy range (that is, $\alpha(\hbar\omega)$ is nearly independent of photon energy), which is substantially larger than the Pt thickness of 3 nm. This suggests that spin generation is relatively uniform throughout the thickness for all investigated photon energies, thereby resulting in minimal photon energy dependence. For Au10Co5, the studied thickness of 10 nm is smaller than L_α (≈15 nm) and L_s (≈35 nm). Consequently, there is minimal spin dephasing occurs before reaching the interface, leading to weak dependence of P_c on the photon energy. From the above discussion, we have determined that η predominantly depends on P_s during the optical orientation process.

The calculation of optical orientation in metals is challenging due to their complex band structures.[15c] Here, we have managed to draw valuable insights by considering both experimental data and theoretical modeling. Based on the experimental data of η and the calculated P_c using the spin diffusion model, we have calculated P_s of Pt and Au with amplitude indicated by the right axis of Figure 4c. We then deduce the P_s spectra under the assumption that P_s follows the same trend as absorption, as depicted by the solid line in Figure 4c. The assumption is underpinned by the fundamental physics involved in both processes. Absorption is the process by which light energy is transferred to the electronic states within a material, resulting in the excitation of electrons. Both optical absorption and optical orientation depend on the optical excitation of electrons. Therefore, we propose that the P_s is influenced by how efficiently a material absorbs light. Simultaneously, as can be observed in Figure 4c, the curves reproduce experimental data effectively. Distinct from other heavy metals like Pt, Ta, and W, Au possesses a notable interband transition bandgap of ≈2.5 eV. For interband transitions, the change in orbital angular momentum (Δl) must still adhere to the electric dipole selection rule of ±1. When circularly polarized light interacts with Au, the angular momentum can be transferred to electrons as they transition from the *s* band to the *p* band. Intraband transitions, where electronic transitions occur within the same energy band and the orbital angular momentum remains constant ($\Delta l = 0$), can also generate spin orientation, for example, through virtual interband transitions considering the spin-orbit splitting of the valence band.[19] However, the probability of inducing spin polarization in Au under circularly polarized light may be lower compared to interband transitions. In the case of Pt, the spread-out and less notable interband transition result in a continuous change in P_s.

Nevertheless, there is a discrepancy for photon energy below 1.5 eV for both Au and Pt, as the deduced η is higher than the experimental data. We speculate that the reason lies in the interface junction between the HM and FM with different work functions.[20] To understand this phenomenon, it is necessary to closely examine the spin transport step. Contrary to conventional spin transport at the HM/FM interface, one must consider the superdiffusive transport behavior of hot carriers at energies higher than the Fermi energy due to laser excitation.[3] The hot carriers undergo scattering during transport and reach the interface with energy ranging from E_F to $E_F + 1.5\ eV$ under an 800 nm pump.[21] Previous first-principles calculations have suggested a decreased transmittance of hot electrons through the interface as the energy decreases.[22] For the spin diffusion calculations, we employed a constant interfacial spin-mixing conductance and did not account for the energy dependence. Moreover, energy dependence provides insight into the dominance of diffusive transport during spin transport. Choi et al. proposed that the mechanism of spin transfer from HM to FM could be either diffusive or drift transport, in which the internal electric field at the interface drives the directional motion of spins.[15c] In a diffusion-dominated process, the spin current is driven by a concentration gradient of the spin-polarized carriers. These carriers, particularly those with low energy, can be scattered at the interface or junction, leading to reduced transmittance. Scattering and recombination processes at the interface can impede the motion of low-energy carriers, making it more difficult for the carriers to cross the interface. In contrast, drift-dominated spin transport is driven by an internal electric field, which can effectively push carriers across the interface or junction. In this case, the transmittance would be less sensitive to carrier energy, as the drift mechanism can help overcome interface-related barriers. To clarify this issue, first-principles calculations of photon energy-dependent optical orientation are needed in future investigations.

We would like to emphasize that Au not only exhibits the highest η but also the greatest absorption under a 400 nm pump (see Figure S4, Supporting Information), resulting in a larger spin current and enhanced control of magnetization compared to Pt that is manifested by the tilt of magnetization of 6×10^{-4} for Au and 5×10^{-5} for Pt (see Figure S6, Supporting Information). This effect can be further enhanced through the optimization of material quality, interface properties, and laser parameters. The potential to induce substantial magnetization changes holds the promise for realizing single-shot helicity-dependent switching of ferromagnetic magnetization,[8] as well as the localized excitation

of spin waves for spin-wave computing applications.[23] Moreover, Au is an excellent plasmonic metal at wavelengths longer than 500 nm (photon energy of 2.5 eV), leading to successful implementation in various optical,[24] magneto-optical,[25] and opto-magnetic devices[26] by utilizing plasmonic resonances. Consequently, the Au/FM structure could be engineered to efficiently write and read magnetization at the same time. These attributes make Au a superior choice compared to other heavy metals in opto-magnetic applications.

3. Conclusion

In summary, we report helicity-driven spin transfer torque in HM (Au and Pt)/FM (Co) heterostructures subject to laser exposure at different wavelengths. Our experimental results reveal three significant observations. First, we have discovered a tenfold enhancement of OSOT quantum efficiency in Au compared to the extensively studied Pt with the same thickness when employing a visible pump. Second, we have experimentally investigated the photon energy-dependent OSOT for the first time and subsequently extracted the optical spin orientation spectra for both Au and Pt. Lastly, the energy-dependent spin transport has been experimentally examined in the OSOT system, suggesting that a high-energy pump is favorable for efficient spin transport. Our experimental findings demonstrate that OSOT in Au/FM heterostructures represents a promising platform for diverse applications, such as all-optical switching of magnetization, spin-wave generation and manipulation, and spintronic terahertz emitters, among others.

4. Experimental Section

Time-Resolved Magneto-Optical Kerr Effect Spectroscopy: In our experimental setup, a mode-locked Ti-sapphire laser with a pulse duration of 200 fs and a repetition rate of 80 MHz was employed. The laser had tunable wavelengths from 800 to 1040 nm. A β-phase barium borate crystal was used to produce second harmonic generation (SHG) with wavelengths from 400 to 520 nm. The fundamental and SHG lasers were used for the pump and probe in a two-color pump-probe geometry. The pump beam was frequency-modulated to 10 MHz using an electro-optical modulator. The use of a 10-MHz high-frequency modulation effectively suppressed the laser intensity noise. However, there was a coherent pick-up signal of 10 MHz from the function generator and the electro-optical modulator driver. To eliminate this background noise, the probe beam was modulated by a 200 Hz frequency through an optical chopper. This double modulation technique could enhance the signal-to-noise ratio of the pump-probe experiment.[27] Both pump and probe beam were focused on the samples using a 20× objective lens in normal incidence geometry. Prior to being directed toward the Wollaston prism and a balanced photodetector for polarization detection, the probe beam passed through an optical filter designed to exclude the pump light. All measurements were conducted under ambient room temperature conditions.

Spin Diffusion Simulation: The transfer matrix method was employed to calculate the absorption profile $a(z)$ used in the spin diffusion equation. The number of photo-excited electrons per unit area in the heavy metal is calculated as: $n_{abs} = \frac{Abs \cdot F_{in}}{\hbar\omega}$, where absorption $Abs = \int_0^{d_{Pt} \text{ or } d_{Au}} a(z)dz$. The number of spin-polarized electrons is calculated as: $n_s = P_s \cdot n_{abs}$. To convert to spin chemical potential, the relation used is:[18] $\mu_s = \frac{n_s}{N_s}$, where N_s is the average spin density of states ($N_s = \frac{N_F}{2}$). To solve the spin diffusion equation, an open boundary condition was applied for the heavy metal/air interface. The heavy metal/ferromagnetic metal interface was connected by spin currents: $J_s = G \cdot \Delta\mu_s$. Here $\Delta\mu_s$ denotes the difference of spin chemical potential between the heavy metal and the ferromagnetic metal, and G is the transverse component spin conductance ($G = \frac{Re\{G_{\uparrow\downarrow}\}}{e^2}$, where $G_{\uparrow\downarrow}$ is the interfacial spin-mixing conductance and e is the elementary charge). The spin chemical potential of Co was set to be zero. Diffusion constant (D) was taken as 2.2×10^{-4} and 9.9×10^{-3} $m^2\ s^{-1}$ for Pt[15c] and Au,[18] respectively. N_F was set to be 1.15×10^{48} and $1.125 \times 10^{47}\ J^{-1}\ m^{-3}$ for Pt[15c] and Au,[18] respectively. The values of $Re\{G_{\uparrow\downarrow}\}$ were 0.6×10^{15} and $0.1 \times 10^{15}\ \Omega^{-1}\ m^{-2}$ for the Pt/Co[15c] and Au/Co[28] structures, respectively. The spin collection efficiency of P_c was calculated by setting P_s to be 1.

Supporting Information

Supporting Information is available from the Wiley Online Library or from the author.

Acknowledgements

Y.L. acknowledges the financial support from the National Science Foundation (DMR-1654192, ECCS-2136168, and DMR-2202268).

Conflict of Interest

The authors declare no conflict of interest.

Data Availability Statement

The data that support the findings of this study are available from the corresponding author upon reasonable request.

Keywords

optical orientation, optical spin-orbit torque, ultrafast spin currents, ultrafast spin transport

Received: July 6, 2023
Revised: September 29, 2023
Published online: October 18, 2023

[1] a) E. Beaurepaire, J.-C. Merle, A. Daunois, J.-Y. Bigot, *Phys. Rev. Lett.* **1996**, *76*, 4250; b) J. Y. Bigot, M. Vomir, *Ann. Phys.* **2013**, *525*; c) A. V. Kimel, M. Li, *Nat. Rev. Mater.* **2019**, *4*, 189; d) C. Wang, Y. Liu, *Nano Converg.* **2020**, *7*, 1.

[2] a) A. Eschenlohr, M. Battiato, P. Maldonado, N. Pontius, T. Kachel, K. Holldack, R. Mitzner, A. Föhlisch, P. M. Oppeneer, C. Stamm, *Nat. Mater.* **2013**, *12*, 332; b) N. Bergeard, M. Hehn, S. Mangin, G. Lengaigne, F. Montaigne, M. Lalieu, B. Koopmans, G. Malinowski, *Phys. Rev. Lett.* **2016**, *117*, 147203.

[3] a) M. Battiato, K. Carva, P. M. Oppeneer, *Phys. Rev. Lett.* **2010**, *105*, 027203; b) M. Battiato, K. Carva, P. M. Oppeneer, *Phys. Rev. B* **2012**, *86*, 024404.

[4] a) T. Kampfrath, M. Battiato, P. Maldonado, G. Eilers, J. Nötzold, S. Mährlein, V. Zbarsky, F. Freimuth, Y. Mokrousov, S. Blügel, M. Wolf, I. Radu, P. M. Oppeneer, M. Münzenberg, *Nat. Nanotechnol.* **2013**, *8*, 256; b) T. J. Huisman, R. V. Mikhaylovskiy, J. D. Costa, F. Freimuth,

E. Paz, J. Ventura, P. P. Freitas, S. Blügel, Y. Mokrousov, T. Rasing, A. V. Kimel, *Nat. Nanotechnol.* **2016**, *11*, 455; c) T. Seifert, S. Jaiswal, U. Martens, J. Hannegan, L. Braun, P. Maldonado, F. Freimuth, A. Kronenberg, J. Henrizi, I. Radu, E. Beaurepaire, Y. Mokrousov, P. M. Oppeneer, M. Jourdan, G. Jakob, D. Turchinovich, L. M. Hayden, M. Wolf, M. Münzenberg, M. Kläui, T. Kampfrath, *Nat. Photonics* **2016**, *10*, 483; d) T. H. Dang, J. Hawecker, E. Rongione, G. Baez Flores, D. Q. To, J. C. Rojas-Sanchez, H. Nong, J. Mangeney, J. Tignon, F. Godel, S. Collin, P. Seneor, M. Bibes, A. Fert, M. Anane, J.-M. George, L. Vila, M. Cosset-Cheneau, D. Dolfi, R. Lebrun, P. Bortolotti, K. Belashchenko, S. Dhillon, H. Jaffrès, *Appl. Phys. Rev.* **2020**, *7*, 041409.

[5] D. Kong, X. Wu, B.o Wang, T. Nie, M. Xiao, C. Pandey, Y. Gao, L. Wen, W. Zhao, C. Ruan, J. Miao, Y. Li, L. Wang, *Adv. Opt. Mater.* **2019**, *7*, 1900487.

[6] a) P. Agarwal, L. Huang, S. Ter Lim, R. Singh, *Nat. Commun.* **2022**, *13*, 4072; b) A. R. Will-Cole, C. Wang, N. Bhattacharjee, Y. Liu, N. X. Sun, *Phy. Rev. B* **2022**, *106*, 174401.

[7] a) A. J. Schellekens, K. C. Kuiper, R. R. J. C. De Wit, B. Koopmans, *Nat. Commun.* **2014**, *5*, 4333; b) G.-M. Choi, C.-H. Moon, B.-C. Min, K.-J. Lee, D. G. Cahill, *Nat. Phys.* **2015**, *11*, 576.

[8] a) J. Igarashi, W. Zhang, Q. Remy, E. Díaz, J.-X. Lin, J. Hohlfeld, M. Hehn, S. Mangin, J. Gorchon, G. Malinowski, *Nat. Mater.* **2023**, *22*, 725; b) Q. Remy, J. Hohlfeld, M. Vergès, Y. Le Guen, J. Gorchon, G. Malinowski, S. Mangin, M. Hehn, *Nat. Commun.* **2023**, *14*, 445.

[9] F. Cheng, Z. Du, X. Wang, Z. Cai, L. Li, C. Wang, A. Benabbas, P. Champion, N. Sun, L. Pan, Y. Liu, *Adv. Opt. Mater.* **2020**, *8*, 2000379.

[10] *Optical Orientation*, (Eds: F. Meier, B. P. Zakharchenya), Elsevier, Amsterdam, The Netherlands **1984**.

[11] a) D. T. Pierce, F. Meier, *Phys. Rev. B* **1976**, *13*, 5484; b) M. D'alessandro, D. Sangalli, *Phys. Rev. B* **2020**, *102*, 104437.

[12] P. Nemec, E. Rozkotová, N. Tesarová, F. Trojánek, E. De Ranieri, K. Olejník, J. Zemen, V. Novák, M. Cukr, P. Malý, T. Jungwirth, *Nat. Phys.* **2012**, *8*, 411.

[13] N. Tesarová, P. Nemec, E. Rozkotová, J. Zemen, T. Janda, D. Butkovicová, F. Trojánek, K. Olejník, V. Novák, P. Malý, T. Jungwirth, *Nat. Photonics* **2013**, *7*, 492.

[14] a) C.-H. Lambert, S. Mangin, B. C. S. Varaprasad, Y. K. Takahashi, M. Hehn, M. Cinchetti, G. Malinowski, K. Hono, Y. Fainman, M. Aeschlimann, E. E. Fullerton, *Science* **2014**, *345*, 1337; b) S. Mangin, M. Gottwald, C.-H. Lambert, D. Steil, V. Uhlíř, L. Pang, M. Hehn, S. Alebrand, M. Cinchetti, G. Malinowski, Y. Fainman, M. Aeschlimann, E. E. Fullerton, *Nat. Mater.* **2014**, *13*, 286.

[15] a) G.-M. Choi, A. Schleife, D. G. Cahill, *Nat. Commun.* **2017**, *8*, 15085; b) J. Li, P. M. Haney, *Phys. Rev. B* **2017**, *96*, 054447; c) G.-M. Choi, J. H. Oh, D.-K. Lee, S.-W. Lee, K. W. Kim, M. Lim, B.-C. Min, K.-J. Lee, H.-W. Lee, *Nat. Commun.* **2020**, *11*, 1482; d) S. Iihama, K. Ishibashi, S. Mizukami, *Nanophotonics* **2020**, *10*, 1169; e) S. Iihama, K. Ishibashi, S. Mizukami, *J. Appl. Phys.* **2022**, *131*, 023901.

[16] a) G. Isella, F. Bottegoni, A. Ferrari, M. Finazzi, F. Ciccacci, *Appl. Phys. Lett.* **2015**, *106*, 232402; b) F. Bottegoni, C. Zucchetti, G. Isella, E. Pinotti, M. Finazzi, F. Ciccacci, *J. Appl. Phys.* **2018**, *124*, 033902; c) C. Zucchetti, F. Bottegoni, G. Isella, M. Finazzi, F. Rortais, C. Vergnaud, J. Widiez, M. Jamet, F. Ciccacci, *Phys. Rev. B* **2018**, *97*, 125203.

[17] M. Isasa, E. Villamor, L. E. Hueso, M. Gradhand, F. Casanova, *Phys. Rev. B* **2015**, *91*, 024402.

[18] K.-H. Ko, G.-M. Choi, *J. Magn. Magn. Mater.* **2020**, *510*, 166945.

[19] S. Tarasenko, E. Ivchenko, V. Bel'kov, S. Ganichev, D. Schowalter, P. Schneider, M. Sollinger, W. Prettl, V. Ustinov, A. Zhukov, *J. Supercond* **2003**, *16*, 419.

[20] a) G. Ramírez-Caballero, J. M. Martínez de la Hoz, P. B. Balbuena, *J. Phys. Chem. Lett.* **2012**, *3*, 818; b) M. Zeng, B. Chen, S. T. Lim, *Appl. Phys. Lett.* **2019**, *114*, 012401.

[21] a) Y. Beyazit, J. Beckord, P. Zhou, J. Meyburg, F. Kühne, D. Diesing, M. Ligges, U. Bovensiepen, *Phys. Rev. Lett.* **2020**, *125*, 076803; b) K. Bühlmann, G. Saerens, A. Vaterlaus, Y. Acremann, *Sci. Rep.* **2020**, *10*, 12632.

[22] W.-T. Lu, Y. Zhao, M. Battiato, Y. Wu, Z. Yuan, *Phys. Rev. B* **2020**, *101*, 014435.

[23] a) S. Muralidhar, R. Khymyn, A. Awad, A. Alemán, D. Hanstorp, J. Åkerman, *Phys. Rev. Lett.* **2021**, *126*, 037204; b) A. V. Chumak, P. Kabos, M. Wu, C. Abert, C. Adelmann, A. Adeyeye, J. Åkerman, F. G. Aliev, A. Anane, A. Awad, *IEEE Trans. Magn.* **2022**, *58*, 1.

[24] a) N. Meinzer, W. L. Barnes, I. R. Hooper, *Nat. Photonics* **2014**, *8*, 889; b) M. L. Brongersma, N. J. Halas, P. Nordlander, *Nat. Nanotechnol.* **2015**, *10*, 25.

[25] a) N. Maccaferri, I. Zubritskaya, I. Razdolski, I.-A. Chioar, V. Belotelov, V. Kapaklis, P. M. Oppeneer, A. Dmitriev, *J. Appl. Phys.* **2020**, *127*, 080903; b) Y. Wu, P. Xie, Q. Ding, Y. Li, L. Yue, H. Zhang, W. Wang, *J. Appl. Phys.* **2023**, *133*, 030902.

[26] a) F. Cheng, C. Wang, Z. Su, X. Wang, Z. Cai, N. X. Sun, Y. Liu, *Nano Lett.* **2020**, *20*, 6437; b) K. Mishra, R. M. Rowan-Robinson, A. Ciuciulkaite, C. S. Davies, A. Dmitriev, V. Kapaklis, A. V. Kimel, A. Kirilyuk, *Nano Lett.* **2022**, *22*, 9773; c) F. Cheng, C. Wang, Y. Xu, W. Ma, Y. Liu, *ACS Photonics* **2023**, *10*, 1259.

[27] M. J. Gomez, K. Liu, J. G. Lee, R. B. Wilson, *Rev. Sci. Instrum.* **2020**, *91*, 023905.

[28] X. Ma, G. Yu, C. Tang, X. Li, C. He, J. Shi, K. L. Wang, X. Li, *Phys. Rev. Lett.* **2018**, *120*, 157204.